Biotecnia
Journal of biological and health sciences
http://biotecnia.unison.mx
Universidad de Sonora
ISSN: 1665-1456

Original Article

Electrospun PMMA/ZnO membranes to improve the photocatalytic degradation of methylene blue using solar irradiation

Membranas electrohiladas de PMMA/ZnO para mejorar la degradación fotocatalítica de azul de metileno utilizando irradiación solar

Rafael Ramírez Bon[1], Osvaldo Campista-Díaz[2], María Mónica Castillo Ortega[3], Kolli Chandra Sekhar Reddy[1], Aime Margarita Gutiérrez Peralta[1], José Ramón Flores León[3], Irela Santos Sauceda[1,3]*

[1] Centro de Investigación y de Estudios Avanzados del IPN, Unidad Querétaro, A.P. 1-798, Querétaro, Qro., México.
[2] Universidad Politécnica de Sinaloa, Higueras Km 3, 82199 Mazatlán, Sinaloa, México.
[3] Departamento de Investigación en Polímeros y Materiales, Universidad de Sonora, C.P. 83 000, Hermosillo, Sonora, México.

ABSTRACT

Electrospun poly (methyl methacrylate) (PMMA) microfibers were combined with ZnO to enhance the photodegradation of dye molecules. The microstructural characteristic of fibrous material used for the decomposition of methylene blue (MB) present in aqueous solutions under dark and sunlight irradiation, was studied using UV-Vis absorption and photoluminescence spectroscopy. The PMMA fibrous membrane was embedded with ZnO particles using the low temperature heat treatment, providing better membrane handling and changing its morphology. The average diameter of fibrous composite varied between 1.5 ± 0.26 to 2.5 ± 0.36 µm, influenced by thermal treatment and ZnO addition. The EDX analysis indicated the presence and homogenous distribution of Zn and O well over on PMMA fibrous; FTIR, DRX and TGA analysis corroborates the presence and composition of ZnO. The dispersion of ZnO in the polymer matrix influences the roughness and contact angle, important characteristics in the degradation of the dye. Dye molecule discoloration with composite PMMA/ZnO fibers was better in the sunlight irradiation (96 % MB degradation) compared with dark conditions (< 2 % MB degradation). The new strategy of material synthesis for photocatalytic activity suitable for treatment for waste water effluents.

Keywords: electrospinning; heat treatment; poly (methyl methacrylate); zinc oxide; dyes descomposition; sunlight.

RESUMEN

Microfibras electrohiladas de PMMA fueron combinadas con ZnO para aumentar la degradación de moléculas de colorantes. Se realizó la evaluación de la eficiencia de descomposición de azul de metileno (AM) en soluciones acuosas bajo irradiación solar, utilizando espectroscopía de absorción UV-Vis y fotoluminiscencia. Las membranas fibrosas de PMMA fueron embebidas con partículas de ZnO utilizando un tratamiento térmico a bajas temperaturas promoviendo mejor manejabilidad y cambios morfológicos. El diámetro promedio de las fibras varía entre 1.5 ± 0.26 a 2.5 ± 0.36 µm, influenciado por el tratamiento térmico y la adición de ZnO. El análisis de EDS indicó la presencia y distribución homogénea de Zn y O sobre las fibras de PMMA, también por FTIR, XRD y análisis de TGA se corroboró la presencia y composición de ZnO. La dispersión de ZnO en la matriz polimérica influye en la rugosidad y ángulo de contacto, características importantes en la degradación de colorantes. La decoloración de la molécula del colorante con fibras de PMMA/ZnO fue mejor ante la irradiación solar (96 % de degradación del AM) comparada con las condiciones en oscuro (< 2 % de degradación de AM). La nueva estrategia de síntesis del material para la actividad fotocatalítica es adecuada para el tratamiento de efluentes de aguas residuales.

Palabras claves: electrohilado; térmico; poli (metil metacrilato); óxido de zinc: descomposición de colorantes; luz solar.

INTRODUCTION

The photocatalytic technique is among the leading advanced oxidation processes (AOPs) for treating contaminated water, where toxic and harmful substances in water can be decomposed or converted into harmless compounds (Fatimah *et al*., 2011; Kusic *et al*., 2006; Nemiwal *et al*., 2021). This feature is one of the key benefits of photocatalysis as compared to the adsorption process, where the contaminant compounds are just removed from water due to their abundant pore sites and high surface area, while in photocatalysis, the presence of active photogenerating species is necessary, which have the capability to activate the degradation process of various organic pollutants under light irradiation. During the pollutant degradation process, free radicals are generated through the reaction with the electrons and holes generated by the light energy in the photocatalyst. These free radicals then degrade pollutants in the water (Nemiwal *et al*., 2021; Bellardita *et al*., 2020).

Among the most promising photocatalyst is ZnO, because it is economical and generates sufficient photocharge under visible light (Heris *et al*., 2023). Therefore, it has been studied for the photocatalytic degradation of both drugs and dyes such as tetracycline, methyl orange, methylene blue, naproxen, and ibuprofen under visible light (Heris *et al*., 2023; Tekin *et al*., 2020; Akhter *et al*., 2023; Murtaza *et al*., 2022). Different studies concluded that ZnO has better photocatalytic degradation efficiency compared to TiO_2 for certain toxic substances under solar irradiation (Štrbac *et al*., 2018;

*Author for correspondence: Irela Santos Sauceda
e-mail: irela.santos@unison.mx;
Received: February 17, 2025
Accepted: March 19, 2025
Published: April 4, 2025

DOI: 10.18633/biotecnia.v27.2587

Fenoll *et al*., 2015; Kansal *et al*., 2008). In addition, different ZnO nanostructures with high surface to volume ratio such as fibers, particles and wires have been studied to improve the degradation efficiency of some toxic compounds (Albiss and Abu-Dalo, 2021; Choudhary *et al*., 2023; Jiang *et al*., 2023; Nagasundari *et al*., 2021; Pantò *et al*., 2021; Vasantharaj *et al*., 2021). Likewise, they have shown difficulty in their handling at the end of the photocatalytic process, causing losses of the photocatalyst (Chen *et al*., 2020; Cordoba *et al*., 2022), therefore preventing the use of these materials at industrial level. In these cases, the immobilization of the photocatlytic materials in the appropriate substrates can be employed to address these issues. The immobilized photocatalysts not only enable their easy recovery from the solution, but also prevents the photocatalyst particles to lose and suspend in the solution producing light dispersion and reducing the light penetration (Cordoba *et al*., 2022; Zakria *et al*., 2021), which reduces the photocatalysis efficiency.

Electrospun polymeric fibers are considered as available candidates for AOPs due to their physical and chemical properties (Cordoba *et al*., 2022). Through the electrospinning technique, it is possible to obtain fibers with diameters in the order of a few microns to tens of nanometers, which provides materials with high specific surface area and high porosity (Lv *et al*., 2023), allowing high concentration of photocatalyzing nanoparticles in the fibers, avoiding agglomeration, and improving the exposure to the light.

PMMA has emerged as a polymer of significant interest due to its remarkable properties, including biocompatibility, mechanical strength, thermal stability, electrical insulation, and high optical transparency. Besides, it can be easily processed by electrospinning. Hybrid composites based on PMMA electrospun fibers supporting inorganic substances such as TiO_2 (Lee *et al*., 2024), Fe_3O_4 (Qi *et al*., 2022), SnO_2/WO_3 (Lin *et al*., 2023), ZnO and Bi_2O_3 (Setayeshi *et al*., 2024), $ZnAl_2O_4$ (Toncelli, 2021), $CsPbI_3$ halide perovskite (Yang *et al*., 2025), have been reported in the literature. Some applications of these hybrid composite materials are lithium-ion batteries, biomedical, photocatalysis, optoelectronic and photovoltaic devices.

PMMA fibrous system with ZnO is of great interest for environmental applications. The previous reports about PMMA fibers with ZnO were focused on scaffolds and antibacterial activity (Saati *et al*., 2024; Setayeshi *et al*., 2024). To our knowledge, the photocatalytic properties of PMMA/ZnO fibers have not been reported yet. The use of this approach for photocatalytical applications of the PMMA fibers with ZnO are explored in this work. We report the preparation of electrospun PMMA fibers with ZnO nanoparticles embedded into the fibers matrix to develop PMM composite fibers with ZnO. By tuning the electrospinning parameters and applying thermal treatment to the electrospun composite fibers, leads to strong chemical bonding between the polymer matrix and the ZnO crystalline phase in the composite fibers structure. Then, the PMMA fibers with ZnO were applied to the photodegradation of methylene blue in aqueous solutions driven by sunlight. The paper includes the analysis of the physical and chemical properties of the PMMA composite fibers with ZnO, as well as the analysis of the MB photodegradation experiments.

MATERIALS AND METHODS

Reagents

The composite membranes were prepared using acetone, obtained from Aldrich. Poly (methyl methacrylate) (PMMA) has a molecular weight of 350,000 g/mol, and ZnO nanopowder (<100 nm partcicle size) was obtained from Sigma-Aldrich.

Preparation of composite fibers by electrospinning

For the preparation of PMMA/ZnO composite fibers, a method similar to that reported by Ohlmaier-Delgadillo *et al*. (2016) was used. First, a 6 wt % polymer solution of PMMA was prepared by dissolving 3 g of PMMA in 50 mL of acetone. The solution was continually magnetic stirred for 24 h at room temperature. Next, 10 wt % and 20 wt % concentrations of ZnO nanopowder (<100 nm particle size) were dispersed in the PMMA solution to obtain the PMMA/ZnO precursor solution for the electrospinning process. Finally, the PMMA solution with ZnO was added to a 5 mL syringe for electrospinning. For this, the solution was pumped (kdScientific) at a 2 mL/h flow, the distance between the collector and the needle tip was 15 cm and a 17 kV voltage was applied with a voltage source (Bertan). The electrospun composite fibers were collected on aluminum foil to form membranes. Subsequently, they underwent a 3-hour heat treatment at 140°C. In Fig.1, the preparation of composite membranes its illustrated.

Characterization of the composite fibers

The morphology of the electrospun fibers was analized by scanning electron microscopy (SEM) using a Philip XL30 ESEM microscope. The membranes surface roughness was measured by a profilometry technique with a Bruker instrument. The elemental mapping and energy-dispersive X-ray spectroscopy (EDX) spectra of the PMMA fibers with ZnO were acquired to determine the presence and distribution of the ZnO nanoparticles in the fiber membrane. The crystalline phases present in the composite fibers were identified using a Rigaku Dmax2100 X-ray diffractometer. Fourier-transform infrared spectroscopy (FTIR) measurements of the composite fibers were obtained with a GX Perkin Elmer spectrometer using the diffuse reflectance configuration from 4000 to 370 cm^{-1} with a resolution of 4 cm^{-1}. The thermal decomposition of the fibers was analyzed by thermogravimetric analysis (TGA) measurements, carried out in a Perkin-Elmer model Pyris 1 using alumina sample holders, with heating rate of 10°C min^{-1}, from room temperature to 800°C under a flow of nitrogen.

Photocatalysis of Methylene Blue

The PMMA composite fibers with ZnO were used for the photocatalytic degradation of MB (Hycel) in aqueous solution.

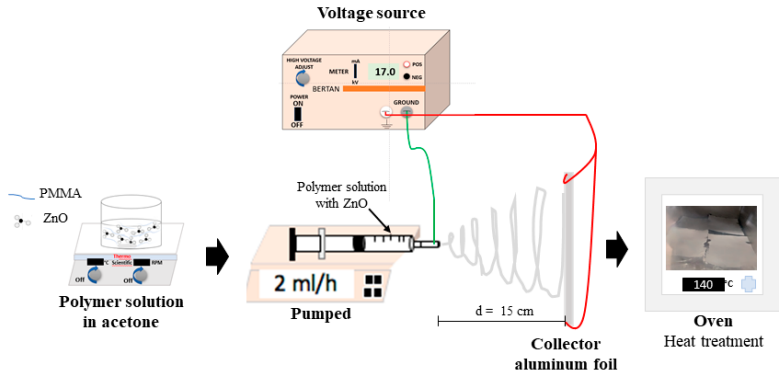

Fig. 1. Schematic diagram of the preparation of composite membranes.
Fig. 1. Diagrama esquemático de la preparación de membranas compuestas.

Initially, an aqueous solution of MB (0.02 mM) was prepared and poured into a 100 mL beaker. Subsequently, a piece of the composite fiber membrane (30 mg) was immersed in the MB solution. Two beakers containing the MB solution, one with the photocatalyst and the other without, were exposed to sunlight irradiation.

To analyze the adsorption of MB on the composite fibers, the experiment was also conducted under dark conditions. The concentration and photodegradation of MB in the aqueous solutions were monitored using UV-visible spectroscopy and spectrofluorimetry at different time intervals (2, 3, 4, and 5 hours), both in darkness and under sunlight irradiation.

The photocatalytic efficiency was determined from the degradation percentage of the MB solution using UV-Vis absorption spectra (Equation 1).

$$Degradation\ (\%) = \left[1 - \frac{C}{C_o}\right] x\ 100 \qquad (1)$$

where *t* is the time the MB solution was exposed to illumination, *Co* and *C(t)* are the MB concentrations at time zero and *t*, respectively. Additionally, the decomposition kinetics of MB was studied by fitting the data to the Langmuir-Hinshelwood model (Equation 2) (Kuo *et al*., 2001). The decomposition kinetics of MB was studied by fitting the data to the Langmuir-Hinshelwood model (Equation 2) (Kuo *et al*., 2001):

$$Ln\ \frac{C}{Co} = -kt \qquad (2)$$

where *k* is the rate constant of the MB photodegradation process. The concentration of the MB solution is obtained from the maximum in the MB absorption bands in the UV-Vis absorption spectra measured as a function of *t*.

RESULTS AND DISCUSSION

The morphology of the electrospun fibers is observed in the SEM micrographs shown in Fig. 2. The PMMA fibers in Fig. 2a) before and 2b) after the heat treatment, display their fibrous characteristics with tens of microns length and ribbon (flat) and cylindrical (round) shape. The histograms to the right of the micrographs correspond to the cylindrical fiber's diameter distribution, showing an average diameter of 2.3 ± 0.51 µm and 1.4 ± 0.27 mm for the PMMA fibers before and after the heat treatment, respectively. That is, the heat treatment reduces the fibers diameter, which could be due to the loss of moisture, reducing the swelling of the fibers. Likewise, more

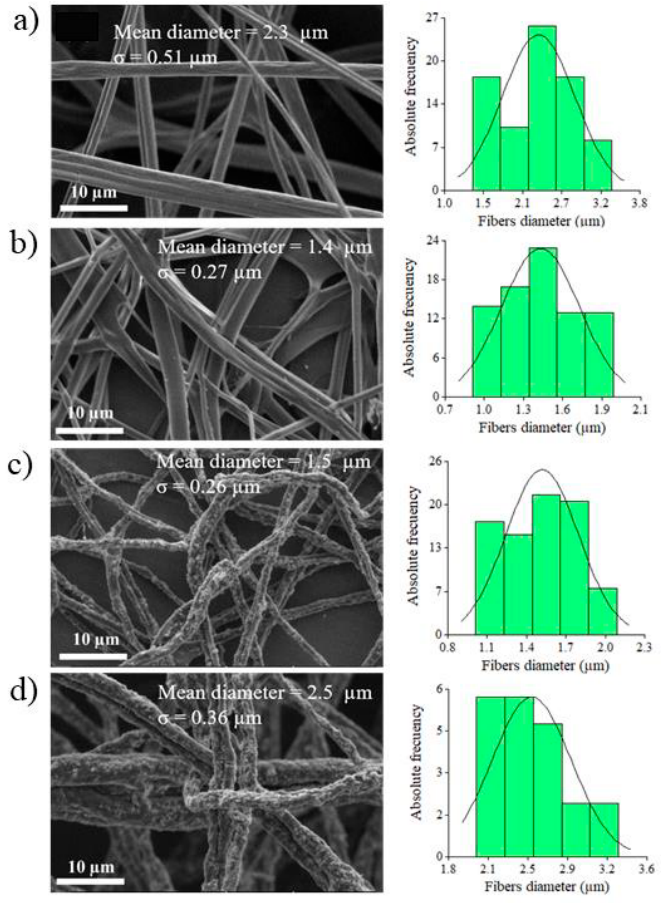

Fig. 2. SEM micrographs and distribution diameter of PMMA fibers, (a) without and (b) with heat treatment, (c) and (d) fibers with 10 wt % and 20 wt % of ZnO, respectively.
Fig.2. Micrografías de SEM y distribución de diámetro de fibras de PMMA, (a) sin y (b) con tratamiento térmico, (c) fibras con 10 % wt y 20 % wt de ZnO, respectivamente.

extended or ribbon-shaped fibers predominate, which is possibly due to the adhesion between the fibers as shown with red arrows in Fig. 2b). This can be attributed to the softening point of PMMA which can change the microporous structure (Ren *et al*., 2023; Carrizales *et al*., 2008). Meanwhile, figures 2c) and 2d) show the PMMA fibers with 10 wt % and 20 wt % of ZnO nanoparticles concentration, respectively. After the addition of the ZnO nanoparticles to the PMMA solution, the electrospun PMMA fibers with ZnO shape looks wrinkled as compared to pure PMMA fibers. This effect is produced by the embedded ZnO nanoparticles, which can be observed protruding in the fibers surface with some agglomeration. For these fibers, the histograms are also shown to the right of the micrographs. The fibers average diameter measured in these histograms were 1.5 ± 0.26 µm and 2.5 ± 0.36 µm, for the PMMA fibers with 10 wt % and 20 wt % of ZnO nanoparticles concentration, respectively. The loading of higher concentration of ZnO nanoparticles increases the diameter of the fibers. This could be due to the increased viscosity of the precursor solution when the ZnO nanoparticles are incorporated. This effect has also been observed for other systems such as PMMA with TiO_2 in DMF (Stoilova *et al*., 2021). The membrane with 10 wt % of ZnO nanoparticles concentration has better homogeneity with respect to diameter of the fibers.

Another important characteristic in the separation process is the roughness of the material. This can help facilitate or prevent the dye molecule contact with active sites of the membrane. Therefore, the profilometry analysis was performed for the heat-treated fiber samples, which are easier to handle and macroscopically look flatter. The profilometry images of the fibers are shown in Fig. 3, where the fibrous morphology for all the samples can be corroborated, in agreement with the SEM images in Fig. 2. The optical images in figures 3a), 3b), and 3c), correspond to the PMMA, PMMA fibers with 10 wt % and 20 wt % of ZnO nanoparticles concentration, respectively. Likewise, the roughness of the fiber membranes determined from these profilometry images is shown in Table 1. The measured roughness in the membranes of PMMA and PMMA with lower ZnO concentration is in the order of a few microns, meanwhile in the PMMA membrane with higher ZnO concentration the roughness increased to around 20 microns. As observed in Fig. 3c), the fibers in the latter membrane are less dense with more empty spaces, which is the cause for the higher roughness, which can decrease the contact of dye molecules with active sites. Similar behavior was shown on casting PMMA films and the addition of TiO_2, where the surface roughness increases drastically from 45 nm to 486 nm while the organic particle concentration increases (Agrawal *et al*., 2020).

Another main characteristic of the fiber membranes applied in separation processes is the water contact angle. The results are also shown in Table 1. The pure PMMA membranes exhibited contact angles of 118.86°, indicating their hydrophobic nature, where the water droplets on the electrospun membrane are quasi-spherical, which greatly reduce

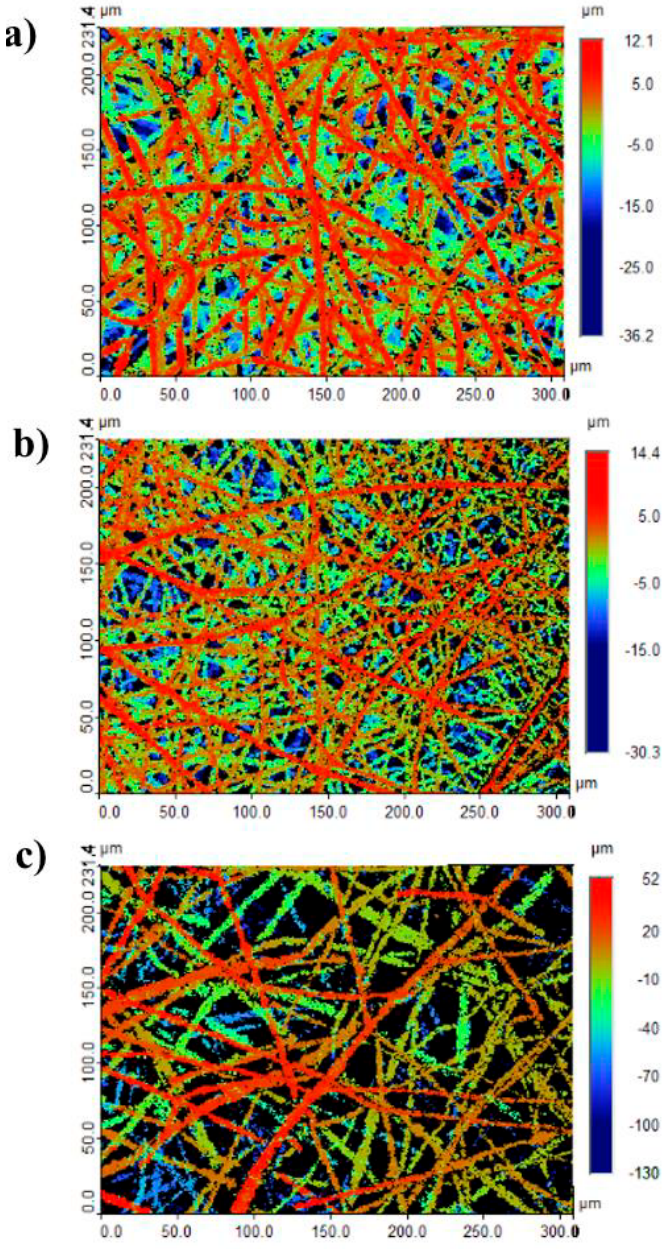

Fig. 3. Profilometry images of membranes a) PMMA, b) PMMA/10 wt % of ZnO and c) PMMA with 20 wt % of ZnO with heat treatment.
Fig. 3. Imágenes de perfilometría de membranas a) PMMA, b) PMMA con 10 % wt de ZnO y c) PMMA con 20% wt de ZnO con tratamiento térmico.

Table 1. Contact angle and roughness of fibrous membranes with heat treatment.
Tabla 1. Ángulo de contacto y rugosidad de membranas fibrosas con tratamiento térmico.

Sample	Roughness (µm)	Contact Angle (°)
PMMA	4.70 ± 0.31	118.66 ± 1.67
PMMA/10%ZnO	3.88 ± 0.70	112.23 ± 1.87
PMMA/20%ZnO	20.14 ± 5.16	114.40 ± 2.01

the contact area between the droplets and the membrane surface (Lu *et al*., 2021). However, the incorporation of ZnO nanoparticles reduced the contact angles to 112.2° and 114.4° for PMMA with 10 wt % and 20 wt % of ZnO, respectively. This suggests an improvement in the wettability of the PMMA membrane with ZnO.

The XRD patterns of the PMMA and PMMA with 10 wt % of ZnO electrospun fibers are shown in Fig. 4. At the top, the pattern of pure PMMA fibers exhibits a broad diffraction band centered around 2θ = 15°, revealing their amorphous characteristics. On the other hand, the pattern of the PMMA with ZnO fibers displays the diffraction peaks of the ZnO hexagonal phase at 31.7°, 34.4°, 36.2°, 47.5°, 56.6°, 62.8°, 66.3, 67.9°, 69°, 72.5° and 76.9°, which are related with the reflections of the (100), (002), (101), (102), (110), (103), (200), (112), (201), (004), and (202) crystalline planes, respectively. The broad diffraction signal of the PMMA phase is also observed with lower intensity in this pattern. In both XRD patterns, the two intense diffraction peaks at 44 and 51 ° are due to the Cu substrate holding the fibers samples. Therefore, this pattern confirms the presence of the ZnO with hexagonal wurtzite structure in the PMMA with ZnO composite fibers. In addition, the clarity of the ZnO signals suggest that there is obtained high cristallinity (Khaleel *et al*., 2023).

With the purpose of studying the effect of the heat treatment and the ZnO addition on PMMA membranes, FITR analysis was done. The FTIR spectra of the PMMA fibers with and without heat treatment, and of the PMMA with 10 wt % of ZnO composite fibers are shown in Fig. 5. The three spectra exhibit the characteristic bands of PMMA within the wavenumber region 3000-2800 cm^{-1} assigned to the C-H stretching vibration of CH_2 and CH_3 groups. The peak at 1730 cm^{-1} corresponds to the C=O stretching vibration of the ester group (Xia *et al*., 2022). The four bands at 1270 cm^{-1}, 1241 cm^{-1}, 1192 cm^{-1} and 1149 cm^{-1} represent the C-O streching vibration of the same ester group (Jafarpour *et al*., 2021; El-

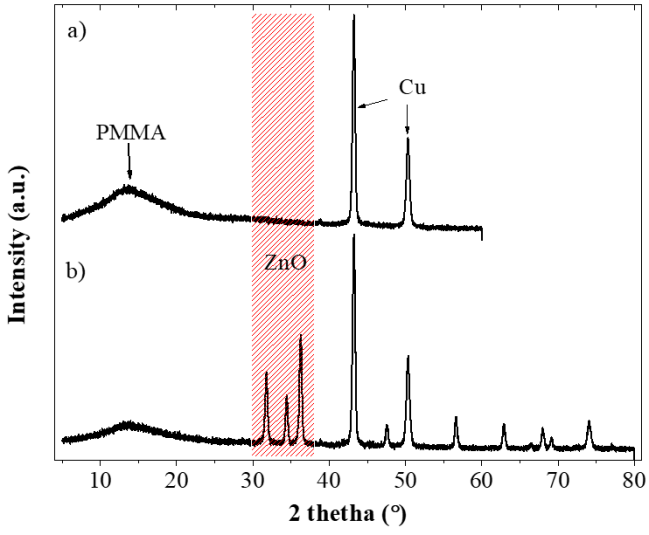

Fig. 4. XRD studies of PMMA fibers a) without and b) with 10 wt % of ZnO.
Fig. 4. Estudios de DRX de fibras de PMMA a) sin y b) con 10% wt de ZnO.

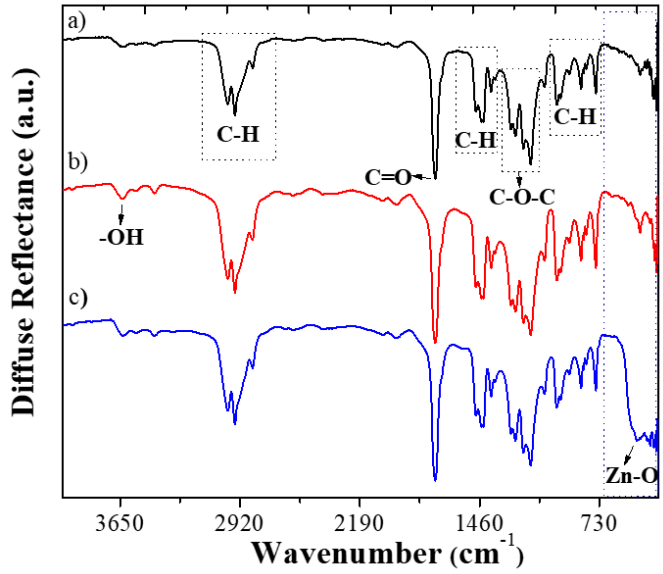

Fig. 5. Diffuse reflectance FTIR spectra of PMMA fibers a) without and b) with heat treatment, and c) PMMA with 10% of ZnO.
Fig. 5. Espectros de FTIR por reflectancia difusa de fibras de PMMA a) sin and b) con tratamiento térmico, y c) PMMA with 10% wt de ZnO.

Sayed and Sayed, 2021). The signals at 1483 cm^{-1}, 841 cm^{-1} and 751 cm^{-1} correspond to the asymmetric bending, symmetric rocking and asymmetric rocking of the -CH_2 group in PMMA, respectively (Xia *et al*., 2022; Matamoros-Ambrocio *et al*., 2021). The bands at 1448 cm^{-1} and 1390 cm^{-1} can be attributed to the C-H asymmetrical and symmetrical bending vibrations of the (–CH_3) methyl group, respectively (Atila *et al*., 2022; Ciulla *et al*., 2023). The band at 1435 cm^{-1} is due to the CH_3 group bending vibrations (Jafarpour *et al*., 2021), while the bands from 1000 cm^{-1} to 900 cm^{-1} correspond to the C-H out of plane bending modes. The spectra of the three fibers samples are very similar regarding the PMMA bands in the wavenumber region from 4000 to 700 cm^{-1}. There are no significant changes in the positions of the signals, only some signals increase or decrease their intensity. On the other hand, in the lower wavenumber range from 700 to 370 cm^{-1}, apparently some signals disappear by the heat treatment, suggesting the possibility of new interactions in the PMMA fibers, responsible for the better integrity of the PMMA fibrous membranes. In the case of the PMMA with ZnO composite fibers spectrum, the band at 502 cm^{-1} corresponds to the Zn-O stretching vibration modes, revealing the presence of the ZnO phase in the composite fibers. This result agrees with was reported for ZnO nanorods (Khan *et al*., 2023).

The TGA measurements of the fibers provided information about their thermal degradation, as well as the interactions between the PMMA and ZnO phases. The results are shown in Fig. 6a) and Fig. 6b) for the PMMA fibrous membranes without and with thermal treatment, respectively, and Fig. 6c) for PMMA with 10 wt % of ZnO and Fig. 6d) for PMMA with 20 wt % of ZnO fibers samples. In the four TGA curves, the initial stage of the degradation begins around 210 °C followed by a strong weight loss starting at 300 °C and

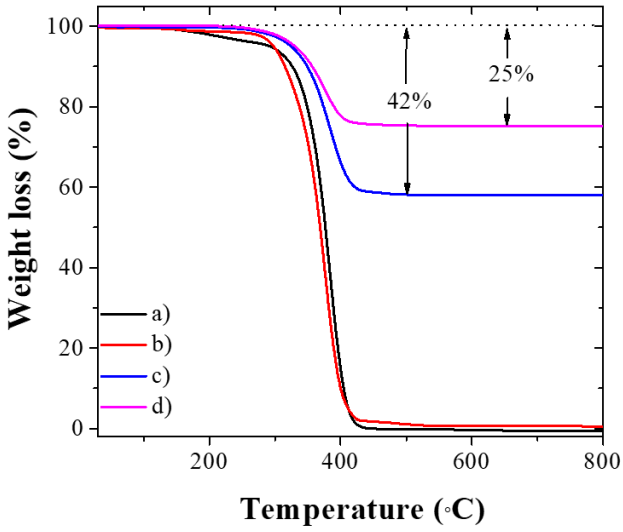

Fig. 6. TGA thermograms of PMMA fibrous membranes without a) and with b) thermal treatment, and for PMMA fibrous membranes with c) 10 wt % ZnO and d) 20 wt % of ZnO.
Fig. 6. Termogramas de TGA de membranas fibrosas de PMMA sin a) y con b) tratamiento térmico, c) y d) para membranas fibrosas de PMMA con 10 % wt de ZnO and 20% wt de ZnO, respectivamente.

ending at 492 °C. Attributed to the residual solvent evaporation, the decomposition of the unsaturated ends from the PMMA chain and its random excision in the main chain of the polymeric membrane without heat treatment, respectively (Lahariya *et al*., 2025). Meanwhile, the thermogram of the membrane subjected to the heat treatment shows better thermal stability. This result is consistent with the FTIR spectrum.

In the case of the PMMA membranes, the weight loss is total and there is not material residue above the temperature of 492 °C, indicating that the organic PMMA was completely decomposed. Meanwhile, in the thermograms of the PMMA with ZnO composite fibers, it can be observed that in the temperature range from 492°C to 800°C, the sample weight stabilizes without significant changes. The final weight of the samples at the highest temperature of 800 °C is 58 % and 75 % of the original weight for the composite fibers with 10 wt % and 20 wt % of ZnO nanoparticles, respectively. That is, the thermal decomposition of the PMMA organic phase in the composite samples left as residual at the highest temperature, influences the content of inorganic ZnO phase in the composite fibers. Since the weight amounts of ZnO phase in the composite are rather high, we can conclude that the electrospinning technique is very appropriate to incorporate high contents of semiconductors nanopowders in the fibrous matrix of PMMA.

Fig. 7 shows the EDX spectra of the PMMA and PMMA fibers with 10 wt % of ZnO. For the spectrum of PMMA fibers only carbon and oxygen are observed as expected (Fig. 7a). Whereas, in the spectrum of PMMA fibers with 10 wt % of ZnO, besides carbon and oxygen (Fig. 7b), the Zn from the ZnO nanoparticles is also detected. Fig. 7c) corresponds to the SEM image of an area of the PMMA fibers with ZnO where the elements mapping by EDX was carried out and shown in Fig. 6 d), e) and f) for the C, O and Zn elements, respectively. The mapping of the Zn element in Fig. 7f) shows the uniform distribution of the ZnO nanoparticles over the PMMA fibers with 10 wt % of ZnO. This is an important characteristic of composite fibers for their photocatalytic applications.

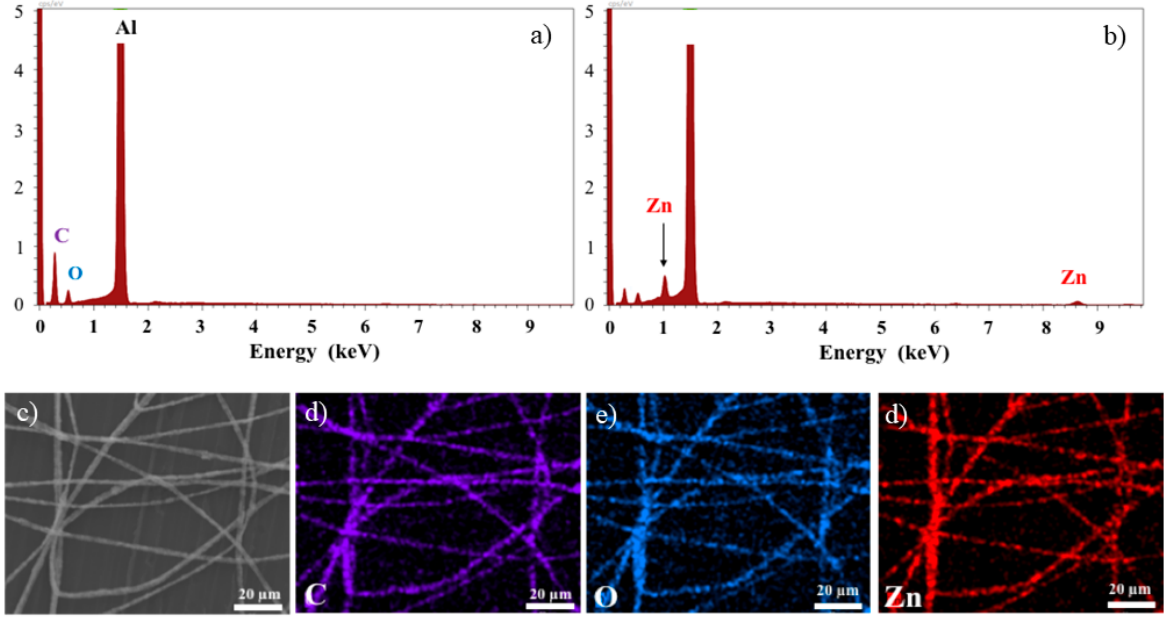

Fig. 7. EDX profiles (a and b), and SEM PMMA with c) 10 wt % of ZnO, d) carbon, e) oxygen and f) zinc mapping of the surfaces.
Fig. 7. Perfiles de EDX (a y b), y c) SEM PMMA with 10% wt de ZnO, mapeo de d) carbono, e) oxígeno y f) zinc de la superficie.

Test of dyes photocatalytic degradation

The photodecoloration efficiency of the MB solutions was studied without and with fibrous material and the results are shown in Fig. 8a). In this plot, to the left of zero time, the results are shown under dark conditions, where no significant changes are observed in the MB solutions, in both cases without and with fibers samples. After exposure to the sunlight, the gradual photodegradation of the MB solutions takes place. After 5 hours the PMMA fibers with concentrations of 10 wt % or 20 wt % of ZnO nanoparticles, achieved 96 % and 90 % of photodegradation, respectively. These results are similar to those obtained for thin ZnO nanofiber films (Aqui-Romero *et al*., 2022).

The composite fibers with lower concentration of ZnO nanoparticles (10 wt %) featured a better percentage of MB degradation than those with higher concentration. This result may be due to the agglomeration of the ZnO nanoparticles in the PMMA matrix at higher concentration, as observed in the SEM and profilometry images. The MB solution without fibers also undergoes some photodegradation when exposed to sunlight, produced by the water photolysis (Khan *et al*., 2022). Finally, the photodegradation trend of the MB solution with the PMMA fibers is practically the same as in the pure MB solution. Therefore, PMMA fibers do not participate in the photodegradation of the MB solution, but water photolysis does.

The photodegradation experimental data were fit to the Langmuir-Hinshelwood equation, and the best fits are shown as solid straight lines in Fig. 8b). The slope of the fitted straight lines represents the rate constant of the photodegradation (k) of the MB solutions. The values of the rate constant k are in the inset of this graph. The PMMA composite membrane with 10 wt % of ZnO has k = 0.0104 min^{-1}, which is three times higher than the corresponding value for the bare PMMA fibers, k = 0.0039 min^{-1}. Similar results have been obtained for the cellulose acetate system with ZnO nanoparticles for the degradation of MB under solar irradiation (k = 0.0114 min^{-1}), which were obtained by phase inversion using dimethylformamide (Abu-Dalo *et al*., 2021).

To compare the photodegradation parameters achieved by the PMMA fibers with ZnO, Table 2 includes the corresponding parameter values for other ZnO-based composite photocatalysts reported in literature. From the values in this table, it can be concluded that the photocatalytic material reported in this work achieved performance parameters comparable and even better than those reported for other ZnO-based composite photocatalysts. Furthermore, the use of natural sunlight is important because it does not generate additional costs, and therefore, is energetically favorable representing an advantage compared to other systems which use UV light sources. Therefore, these results show that the electrospun polymer fibers as the matrix for semiconductor photocatalysts such as ZnO nanoparticles are excellent

Table 2. Comparison of the degradation efficiency of MB with other photocatalytic materials.
Tabla 2. Comparación de la eficiencia de degradación de AM con otros materiales fotocatalíticos.

Sample	Degradation efficiency (%)	Experimental conditions	Light source	Composite form
PANI/ZnO	97	Catalyst= 0.4 mg mL^{-1} [MB]= 1X10^{-5} M Irradiation time=5 hr	UV lamp (254 nm), Sunlight	Sheet-like (Eskizeybek *et al*., 2012)
PMMA-ZnO	~ 62 ~35	Catalyst= 50 mg mL^{-1} MB [MB]= 1.5x10^{-5} M Irradiation time=4 hr	UV lamp (368 nm)	Powders, flat film (Di Mauro *et al*., 2017)
ZnO-PMMA	99	Catalyst= 80 mg/15ml [MB]= 2 mg L^{-1}	Sunlight	Spherical (Rani and Shanker 2018)
ZnO-coated cellulosic	~ 60	[MB] = 1.0x10^{-5} M Irradiation time= 8 hr	UV-Vis lamps	Powder and fibers (Moafi *et al*., 2011)
PMMA/ZnO	96	Catalyst =10 mg/30 ml MB [MB]= 2.0x10^{-5} M Irradiation time = 5 hr	Sunlight	Fibers [In this work]

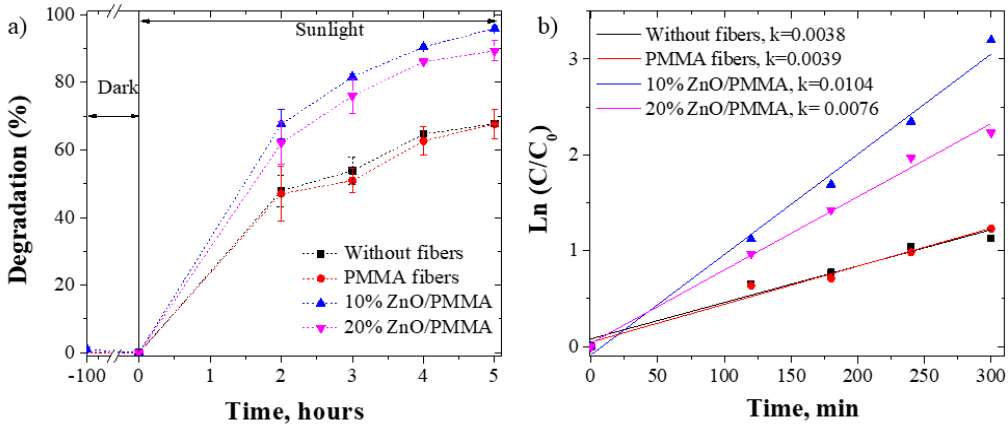

Fig. 8. a) Photocatalitic efficiency and b) kinetic study of MB.
Fig. 8. a) Eficiencia fotocatalítica y b) estudios cinéticos de AM.

alternative to achieve high performance semiconductor composite photocatalysts.

Photoluminiscence analysis of the photodegraded MB solutions was carried out to further investigate the degradation process of MB molecules. The results are shown in Fig. 9, where the emission spectra of the MB aqueous solutions, excited with light of 500 nm, under dark and after exposed to sunlight at different times are plotted. In Fig. 9a), the emission spectrum of the MB solution before degradation (0 h) displays an emission band at 690 nm, which is characteristic of MB. In dark conditions, the emission spectra of the MB solutions almost do not modify, in agreement with absorption measurements. The MB photodegradation by the photolysis mechanism is observed in Fig. 9b), where the emission band at 690 nm gradually decreases its intensity with the time under exposition to sunlight. In addition, a new emission broader band appears at 600 nm, which can be attributed to the formation of subproducts from MB generated by the photolysis process. This behavior is in accordance with the studies done with cellulose acetate fibers for the photodecolorization of methylene blue solutions under natural sunlight (Santos-Sauceda *et al*., 2021). The photocatalytic degradation of MB effects on the emission spectra can be seen in Fig. 9c). Unlike photolysis effects, here the decrease of the emission band intensity is stronger, also in agreement with absorption measurements, and the center of the emission band shifts to lower wavelength. This photoluminescence behavior confirms the contribution of the PMMA composite with ZnO photocatalyst in the photodegradation of the MB substance.

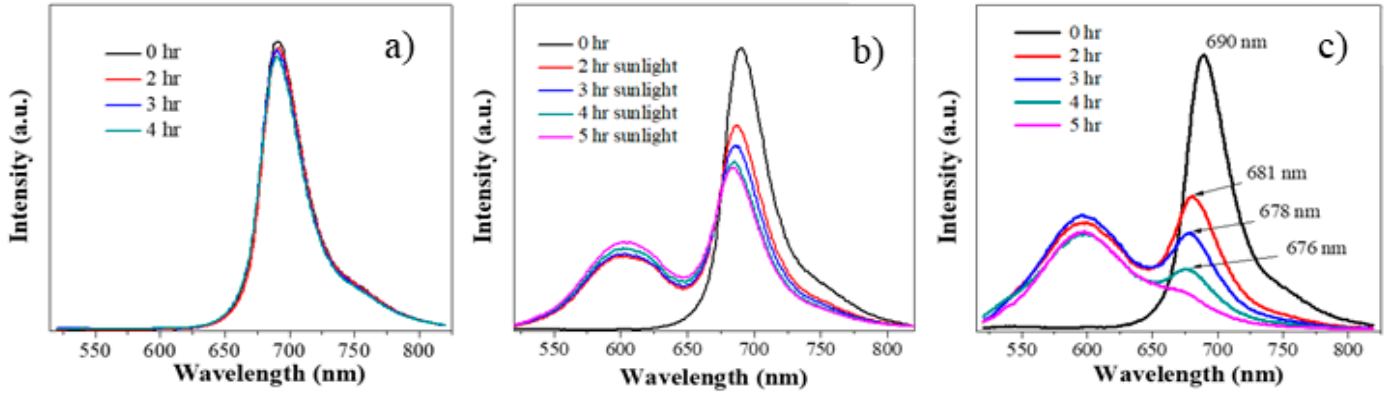

Fig. 9. Emission spectra of MB aqueous solutions in a) conditions dark and b) sunlight without membranes, and c) with PMMA membranes and 10 wt % of ZnO.
Fig. 9. Espectro de emisión de soluciones acuosas de AM en (a) condiciones oscuras y (b) con luz solar sin membranas, y (c) con membranas de PMMA con 10% wt de ZnO.

CONCLUSIONS

PMMA fibrous membranes, with and without ZnO nanoparticles at two different wt %, were prepared by electrospinning where the heating treatment improves the handling and quality of the fibrous material. The incorporation of ZnO nanoparticles in the PMMA electrospun fibers was corroborated by XRD and FTIR measurements and their embedding and uniform distribution in the polymeric fibers by SEM images and EDS elemental mapping. Both types of ZnO-PMMA nanocomposites achieved high % degradation of the MB solutions at 96 % of degradation, and 90 % after 5 h exposed to sunlight. However, the lower % degradation corresponded to the nanocomposites with the higher ZnO (20 wt %) due to nanoparticle agglomeration. On the other hand, the nanocomposites with 10 wt % of ZnO achieved the 96 % of degradation. These photodegradation parameters are comparable to others reported in literature for ZnO-based nanocomposites. Therefore, the electrospun system reported here, PMMA with ZnO, is a good alternative as photocatalytic material for pollutant degradation in contaminated water.

ACKNOWLEDGMENTS

The authors thank to M.I. Adair Jimenez Nieto, M.C. Reina Araceli Mauricio Sánchez, Dr. Damian Plascencia and M.T. Rivelino Flores Farias for his assistance in the analysis morphology by SEM, FTIR, TGA, UV-Vis and photoluminescence spectroscopies studies, respectively.

CONFLICTS OF INTEREST

The authors declare that they have no conflict of interest.

REFERENCES

Abu-Dalo, M.A., Al-Rosan, S.A. and Albiss, B.A. 2021. Photocatalytic degradation of methylene blue using polymeric membranes based on cellulose acetate impregnated with ZnO nanostructures. Polymers, 13(19), 3451.

Agrawal, N.K., Agarwal, R. and Agarwal, P. 2020. Tuning of TiO_2 nanoparticles incorporation in poly methyl methacrylate for synthesis of polymer nanocomposites for promising biomedical application. Materials Today: Proceedings, 30, 137-144.

Akhter, P., Nawaz, S., Shafiq, I., Nazir, A., Shafique, S., Jamil, F. and Hussain, M. 2023. Efficient visible light assisted photocatalysis using ZnO/TiO_2 nanocomposites. Molecular Catalysis, *535*, 112896.

Albiss, B. and Abu-Dalo, M. 2021. Photocatalytic degradation of methylene blue using zinc oxide nanorods grown on activated carbon fibers. Sustainability, 13(9), 4729.

Atila, D., Hasirci, V. and Tezcaner, A. 2022. Coaxial electrospinning of composite mats comprised of core/shell poly (methyl

methacrylate)/silk fibroin fibers for tissue engineering applications. Journal of the Mechanical Behavior of Biomedical Materials, 128, 105105.

Aqui-Romero, F., Santos-Sauceda, I. and Ramirez-Bon, R. 2022. Electrospun ZnO nanofibers thin films for the methylene blue degradation driven by natural sunlight. Inorganic Chemistry Communications, 145, 109962.

Bellardita, M., Camera-Roda, G., Loddo, V., Parrino, F. and Palmisano, L. 2020. Coupling of membrane and photocatalytic technologies for selective formation of high added value chemicals. Catalysis Today, 340, 128-144.

Carrizales, C., Pelfrey, S., Rincon, R., Eubanks, T.M., Kuang, A., McClure, M.J. and Macossay, J. 2008. Thermal and mechanical properties of electrospun PMMA, PVC, Nylon 6, and Nylon 6, 6. Polymers for Advanced Technologies, 19(2), 124-130.

Chen, D., Cheng, Y., Zhou, N., Chen, P., Wang, Y., Li, K. and Ruan, R. 2020. Photocatalytic degradation of organic pollutants using TiO_2-based photocatalysts: A review. Journal of Cleaner Production, 268, 121725.

Choudhary, S., Sharma, M., Krishnan, V. and Mohapatra, S. 2023. Facile synthesis of Ce doped ZnO nanowires for efficient photocatalytic removal of organic pollutants from water. Materials Today Communications, 34, 105361.

Ciulla, M., Canale, V., Wolicki, R.D., Pilato, S., Bruni, P., Ferrari, S. and Di Profio, P. 2023. Enhanced CO_2 capture by sorption on electrospun poly (methyl methacrylate). Separations, 10(9), 505.

Cordoba, A., Saldias, C., Urzúa, M., Montalti, M., Guernelli, M., Focarete, M.L. and Leiva, A. 2022. On the versatile role of electrospun polymer nanofibers as photocatalytic hybrid materials applied to contaminated water remediation: A brief review. Nanomaterials, 12(5), 756.

Di Mauro, A., Cantarella, M., Nicotra, G., Pellegrino, G., Gulino, A., Brundo, M.V. and Impellizzeri, G. 2017. Novel synthesis of ZnO/PMMA nanocomposites for photocatalytic applications. Scientific reports, 7(1), 40895.

Eskizeybek, V., Sarı, F., Gülce, H., Gülce, A. and Avcı, A. 2012. Preparation of the new polyaniline/ZnO nanocomposite and its photocatalytic activity for degradation of methylene blue and malachite green dyes under UV and natural sun lights irradiations. Applied Catalysis B: Environmental, 119, 197-206.

El-Sayed, S. and Sayed, A. M. E. 2021. Preparation and characterization of CuO/Co_3O_4/poly (methyl methacrylate) nanocomposites for optical and dielectric applications. Journal of Materials Science: Materials in Electronics, 32(10), 13719-13737.

Fatimah, I., Wang, S. and Wulandari, D. 2011. ZnO/montmorillonite for photocatalytic and photochemical degradation of methylene blue. Applied Clay Science, *53*(4), 553-560.

Fenoll, J., Vela, N., Garrido, I., Navarro, G., Pérez-Lucas, G. and Navarro, S. 2015. Reclamation of water polluted with flubendiamide residues by photocatalytic treatment with semiconductor oxides. Photochemistry and Photobiology, 91(5), 1088-1094.

Heris, S.Z., Etemadi, M., Mousavi, S.B., Mohammadpourfard, M. and Ramavandi, B. 2023. Preparation and characterizations of TiO_2/ZnO nanohybrid and its application in photocatalytic degradation of tetracycline in wastewater. Journal of Photochemistry and Photobiology A: Chemistry, *443*, 114893.

Jafarpour, M., Aghdam, A.S., Koşar, A., Cebeci, F.Ç. and Ghorbani, M. 2021. Electrospinning of ternary composite of PMMA-PEG-SiO_2 nanoparticles: Comprehensive process optimization and electrospun properties. Materials Today Communications, 29, 102865.

Jiang, Z., Liu, B., Yu, L., Tong, Y., Yan, M., Zhang, R. and Li, W. 2023. Research progresses in preparation methods and applications of zinc oxide nanoparticles. Journal of Alloys and Compounds, 956, 170316.

Kansal, S.K., Singh, M. and Sud, D. 2008. Studies on TiO_2/ZnO photocatalysed degradation of lignin. Journal of Hazardous materials, 153(1-2), 412-417.

Khaleel, A.K. and Abbas, L.K. 2023. Synthesis and characterization of PVDF/PMMA/ZnO hybrid nanocomposite thin films for humidity sensor application. Optik, 272, 170288.

Khan, A., Kamal, T., Saad, M., Ameen, F., Bhat, S.A., Khan, M.A. and Rahman, F. 2023. Synthesis and antibacterial activity of nanoenhanced conjugate of Ag-doped ZnO nanorods with graphene oxide. Spectrochimica Acta Part A: Molecular and Biomolecular Spectroscopy, 290, 122296.

Khan, I., Saeed, K., Zekker, I., Zhang, B., Hendi, A.H., Ahmad, A. and Khan, I. 2022. Review on methylene blue: Its properties, uses, toxicity and photodegradation. Water, 14(2), 242.

Kuo, W.S. and Ho, P.H. 2001. Solar photocatalytic decolorization of methylene blue in water. Chemosphere, 45(1), 77-83.

Kusic, H., Koprivanac, N. and Srsan, L. 2006. Azo dye degradation using Fenton type processes assisted by UV irradiation: A kinetic study. *Journal of Photochemistry and photobiology A:* Chemistry, *181*(2-3), 195-202.

Lahariya, V., Sharma, T. and Behl, S. 2025. Study on the structural, dielectric and thermal degradation of poly (methyl methacrylate)-ZnO nanocomposites. Solid State Communications, 397, 115823.

Lee, J., Yoon, J. and Oh, S.G. 2024. Electrospun nanofiber-based tri-layer separators with CuO/TiO_2 nanowires for high-performance and long-cycle stability of lithium-ion batteries. Journal of Industrial and Engineering Chemistry, 135, 165-174.

Lin, T.H., Chang, Y.H., Hsieh, T.H., Huang, Y.C. and Wu, M.C. 2023. Electrospun SnO_2/WO_3 heterostructure nanocomposite fiber for enhanced acetone vapor detection. Polymers, 15(21), 4318.

Lu, N., Hu, Z., Wang, F., Yan, L., Sun, H., Zhu, Z. and Li, A. 2021. Superwetting electrospun PDMS/PMMA membrane for PM2. 5 capture and microdroplet transfer. Langmuir, 37(44), 12972-12980.

Lv, H., Liu, Y., Bai, Y., Shi, H., Zhou, W., Chen, Y. and Yu, D. G. 2023. Recent combinations of electrospinning with photocatalytic technology for treating polluted water. Catalysts, *13*(4), 758.

Matamoros-Ambrocio, M., Sánchez-Mora, E., Gómez-Barojas, E. and Luna-López, J.A. 2021. Synthesis and study of the optical properties of PMMA microspheres and opals. Polymers, 13(13), 2171.

Moafi, H.F., Shojaie, A.F. and Zanjanchi, M.A. 2011. Photocatalytic self-cleaning properties of cellulosic fibers modified by nano-sized zinc oxide. Thin Solid Films, 519(11), 3641-3646.

Murtaza, S.Z., Shomal, R., Sabouni, R. and Ghommem, M. 2022. Facile metal organic framework composites as photocatalysts for lone/simultaneous photodegradation

of naproxen, ibuprofen and methyl orange. Environmental Technology & Innovation, 27, 102751.

Nagasundari, S.M., Muthu, K., Kaviyarasu, K., Al Farraj, D.A. and Alkufeidy, R.M. 2021. Current trends of Silver doped Zinc oxide nanowires photocatalytic degradation for energy and environmental application. Surfaces and Interfaces, 23, 100931.

Namouchi, F., Smaoui, H., Fourati, N., Zerrouki, C., Guermazi, H. and Bonnet, J. J. 2009. Investigation on electrical properties of thermally aged PMMA by combined use of FTIR and impedance spectroscopies. Journal of Alloys and Compounds, 469(1-2), 197-202.

Nemiwal, M., Zhang, T.C. and Kumar, D. 2021. Recent progress in g-C_3N_4, TiO_2 and ZnO based photocatalysts for dye degradation: Strategies to improve photocatalytic activity. Science of the total environment, 767, 144896.

Ohlmaier-Delgadillo, F., Castillo-Ortega, M.M., Ramírez-Bon, R., Armenta-Villegas, L., Rodríguez-Félix, D.E., Santacruz-Ortega, H., ... and Santos-Sauceda, I. 2016. Photocatalytic properties of PMMA-TiO_2 class I and class II hybrid nanofibers obtained by electrospinning. Journal of Applied Polymer Science, 133(48).

Pantò, F., Dahrouch, Z., Saha, A., Patanè, S., Santangelo, S. and Triolo, C. 2021. Photocatalytic degradation of methylene blue dye by porous zinc oxide nanofibers prepared via electrospinning: When defects become merits. Applied Surface Science, 557, 149830.

Qi, H., Wang, G., Hu, Y., Shao, H., Ma, Q., Li, D. and Dong, X. 2022. Conjugate electro-spinning towards Janus nanofibers array synchronously endowed with conductive anisotropy, magnetism and luminescence. Materials Today Communications, 33, 104765.

Rani, M. and Shanker, U. 2018. Sun-light driven rapid photocatalytic degradation of methylene blue by poly (methyl methacrylate)/metal oxide nanocomposites. Colloids and Surfaces A: Physicochemical and Engineering Aspects, 559, 136-147.

Ren, G., Li, Z., Tian, L., Lu, D., Jin, Y., Zhang, Y. and Sun, D. 2023. Environmentally friendly waterproof and breathable electrospun nanofiber membranes via post-heat treatment. Colloids and Surfaces A: Physicochemical and Engineering Aspects, 658, 130643.

Saati, S.A., Kadhim, Q.S., Mahdi, A.A.A. and Alfalluji, A.L. 2024. Electrospinning for Creation of Zinc Oxide/Poly (methyl methacrylate) Nanofiber Scaffolds. In IOP Conference Series: Earth and Environmental Science (Vol. 1325, No. 1, p. 012045). IOP Publishing.

Santos-Sauceda, I., Castillo-Ortega, M.M., del Castillo-Castro, T., Armenta-Villegas, L. and Ramírez-Bon, R. 2021. Electrospun cellulose acetate fibers for the photodecolorization of methylene blue solutions under natural sunlight. Polymer Bulletin, 78, 4419-4438.

Setayeshi, S., Motakef Kazemi, N. and Ziyadi, H. 2024. Fabrication and characterization of poly (methyl methacrylate) composite nanofibers incorporated with zinc oxide and bismuth oxide nanoparticles and investigation of antibacterial activity. *Polymer Bulletin*, *81*(12), 10897-10914.

Stoilova, O., Manolova, N. and Rashkov, I. 2021. Electrospun poly (methyl methacrylate)/TiO_2 composites for photocatalytic water treatment. Polymers, 13(22), 3923.

Štrbac, D., Aggelopoulos, C.A., Štrbac, G., Dimitropoulos, M., Novaković, M., Ivetić, T. and Yannopoulos, S.N. 2018. Photocatalytic degradation of Naproxen and methylene blue: Comparison between ZnO, TiO_2 and their mixture. Process Safety and Environmental Protection, *113*, 174-183.

Tekin, D., Kiziltas, H. and Ungan, H. 2020. Kinetic evaluation of ZnO/TiO_2 thin film photocatalyst in photocatalytic degradation of Orange G. Journal of Molecular Liquids, 306, 112905.

Toncelli, A. 2021. Re-based inorganic-crystal nanofibers produced by electrospinning for photonic applications. Materials 2021, 14, 2679.

Vasantharaj, S., Sathiyavimal, S., Senthilkumar, P., Kalpana, V.N., Rajalakshmi, G., Alsehli, M. and Pugazhendhi, A. 2021. Enhanced photocatalytic degradation of water pollutants using bio-green synthesis of zinc oxide nanoparticles (ZnO NPs). Journal of Environmental Chemical Engineering, 9(4), 105772.

Yang, H., Li, K., Ji, Y., Lin, D., Shih, W.Y. and Shih, W.H. 2025. Sodium doped $CsPbI_3$-PMMA composite electrospun fibrous membranes for aqueous photocatalyst and LED. Materials Science and Engineering: B, 312, 117835.

Xia, J., Zheng, Z. and Guo, Y. 2022. Mechanically and electrically robust, electro-spun PVDF/PMMA blend films for durable triboelectric nanogenerators. Composites Part A: Applied Science and Manufacturing, 157, 106914.

Zakria, H.S., Othman, M.H.D., Kamaludin, R., Kadir, S.H.S.A., Kurniawan, T.A. and Jilani, A. 2021. Immobilization techniques of a photocatalyst into and onto a polymer membrane for photocatalytic activity. RSC advances, 11(12), 6985-7014.